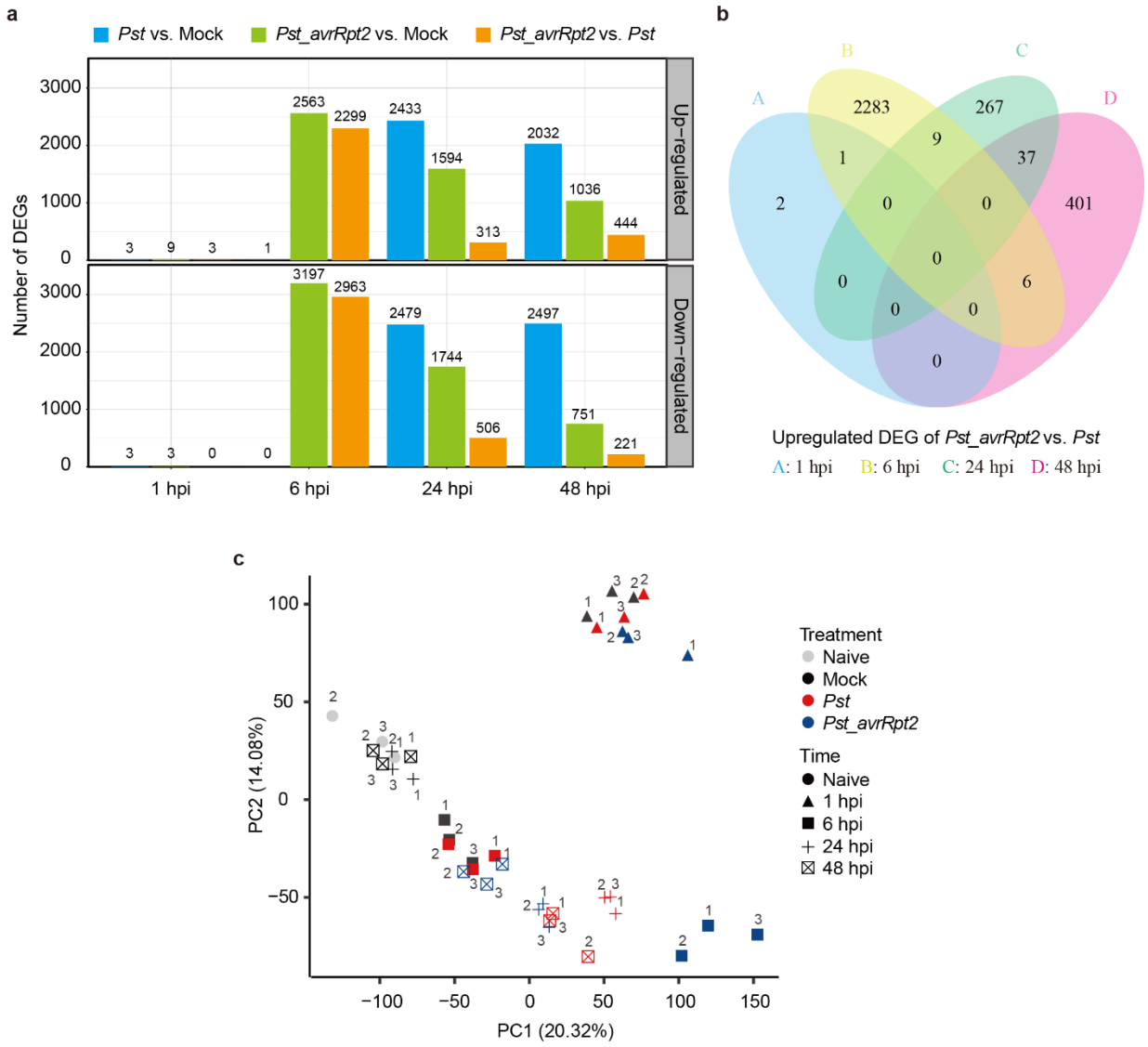

Supplementary Fig. 1 | Transcriptome dynamics in *Pst*- and *Pst_avrRpt2*-inoculated Arabidopsis. RNA-seq was performed on WT Arabidopsis at 1, 6, 24, and 48 hpi with *Pst*, *Pst_avrRpt2* or buffer (mock); no treatment (naive) was used as a control (0 hpi). **a,** DEGs between the indicated treatment pairs at the indicated times; upregulated (upper) and downregulated (lower). **b,** Overlap of upregulated DEGs in *Pst*- and *Pst_avrRpt2*-inoculated WT at 1, 6, 24, and 48 hpi. **c,** Principal component analysis of the normalized RNA-seq data.

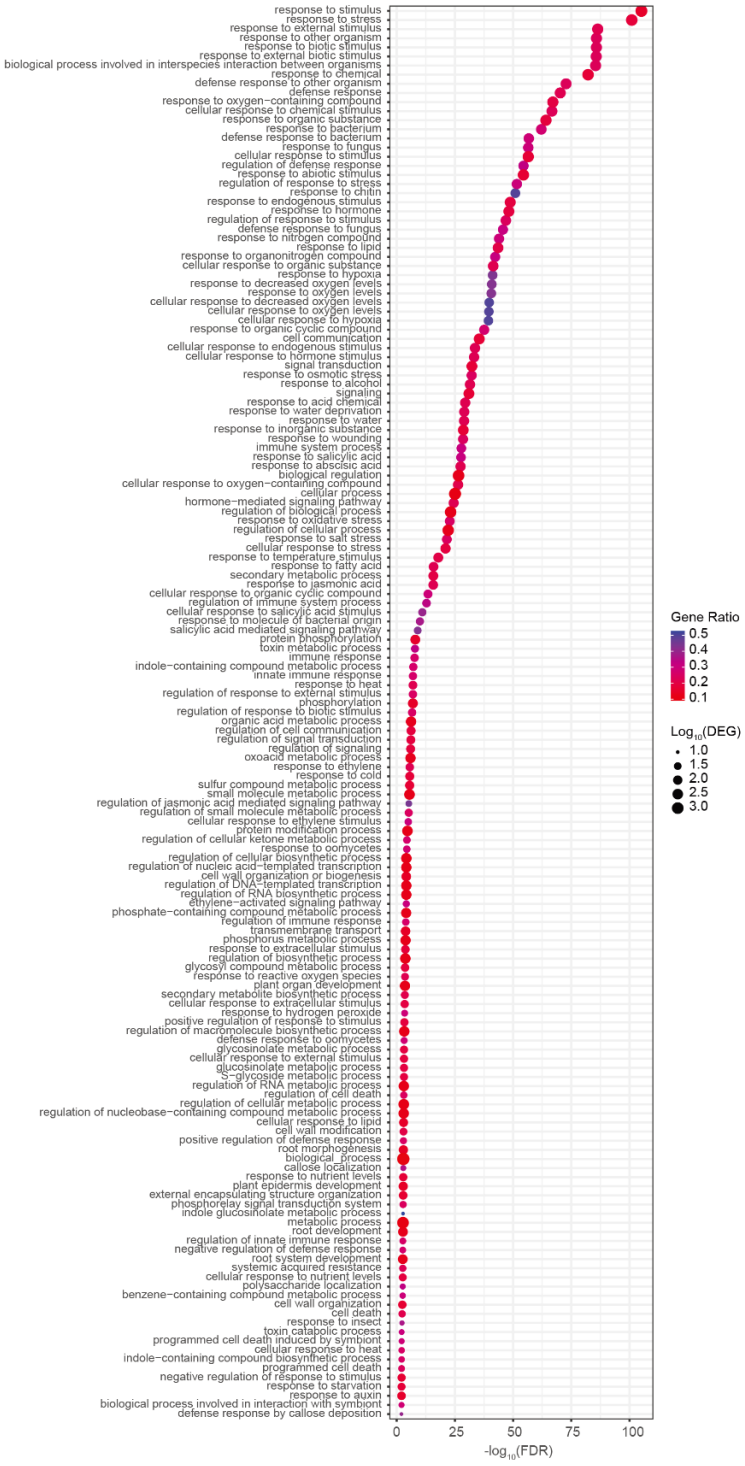

Supplementary Fig. 2 | Gene ontology analysis of ETI-DEGs. GO enrichment analysis ("biological process" category) of ETI up-regulated genes using Fisher's exact test. x-axis: adjusted P-value (FDR, false discovery rate); y-axis: enriched GO term. Dots represent term significantly enriched terms. Gene ratio (#significant genes / #annotated genes) indicating the statistical significance of the enrichment is represented along a gradient color from blue (less significant) to red (most significant). The sizes of the dots represent the count of DEGs belonging to each term. Only the significantly enriched GO categories (FDR < 0.01) are presented.

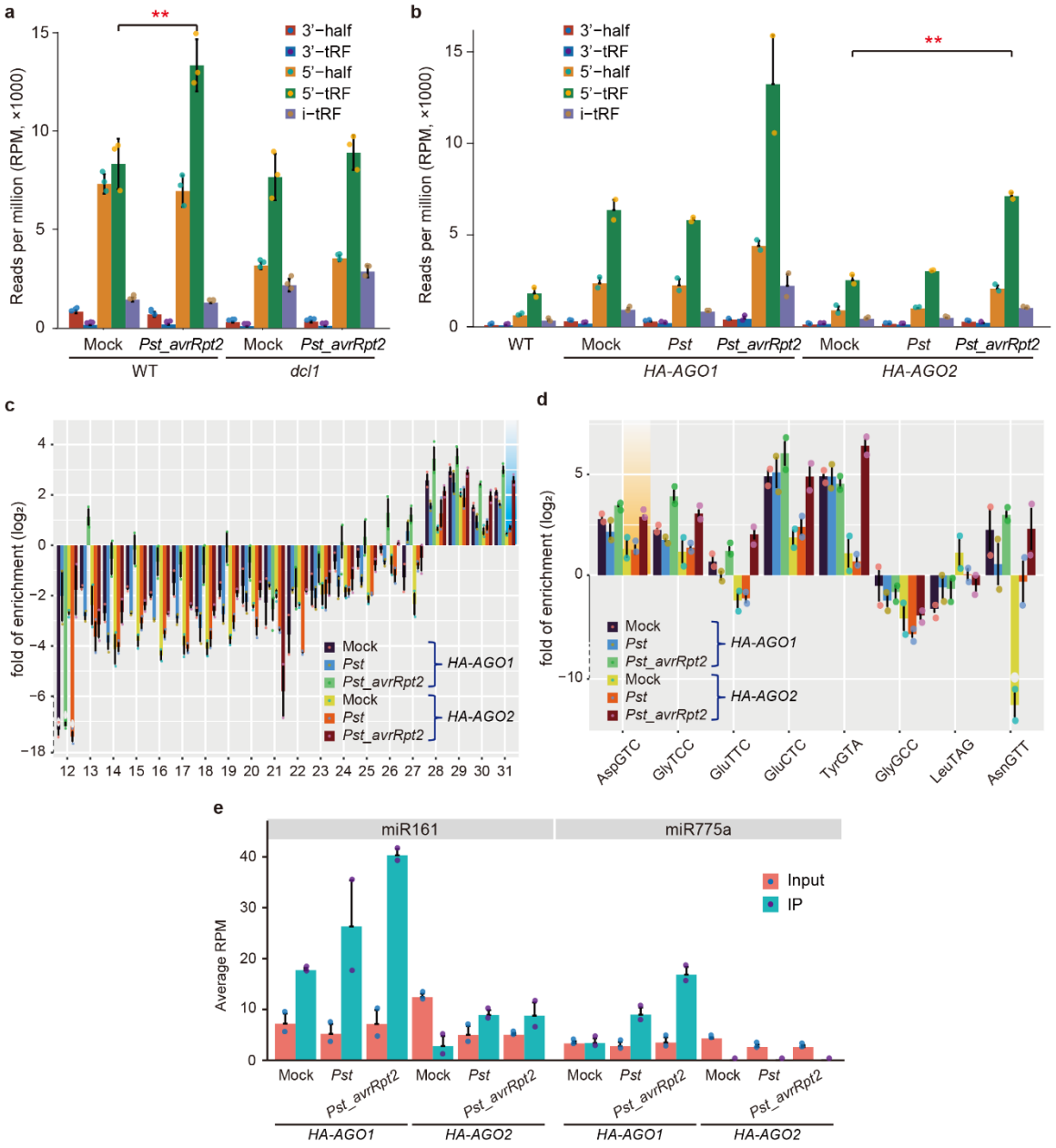

Supplementary Fig. 3 | 5'-tRFs are the dominant tRNA-derived and AGO1/2-associated sRNAs in the nucleus. a, Relative abundance of the different tsRNA classes in the nucleus of *Pst_avrRpt2*- and mock-inoculated WT and *dcl1-7* at 1 hpi. **b,** Relative abundance of the different tsRNA classes in nuclear sRNAs recovered from *HA-AGO1* and *HA-AGO2* transgenic Arabidopsis following α-HA immunoprecipitation. WT was used as one of the negative controls for immunoprecipitation. Statistical difference between indicated pairs is noted; **P<0.01 (*t*-test). **c and d**, Fold enrichment of nuclear AGO1- and AGO2-bound 5'-tRFs in response to *Pst* or *Pst_AvrRpt2* infection relative to their corresponding input. AGO1/2-bound sRNAs and their input sRNAs were normalized as RPM. The y-axis shows the fold enrichment (AGO-bound/Input) on a log2 scale. In panel c, the x-axis represents the sizes of 5'-tRFs, while in panel d, it corresponds to the 5'-tRFs shown in Figure 2e. Statistical differences between the pairs highlighted in Figures 2d and 2e are indicated with an asterisk (P < 0.05; t-test). **e**, Quantification of known AGO1-bound microRNAs in RIP-seq reads. miR161 (left) is known to preferentially associate with AGO1, while miR775a (right) is AGO1-specific. The y-axis represents the mean ± SE (n=2) of the corresponding reads.

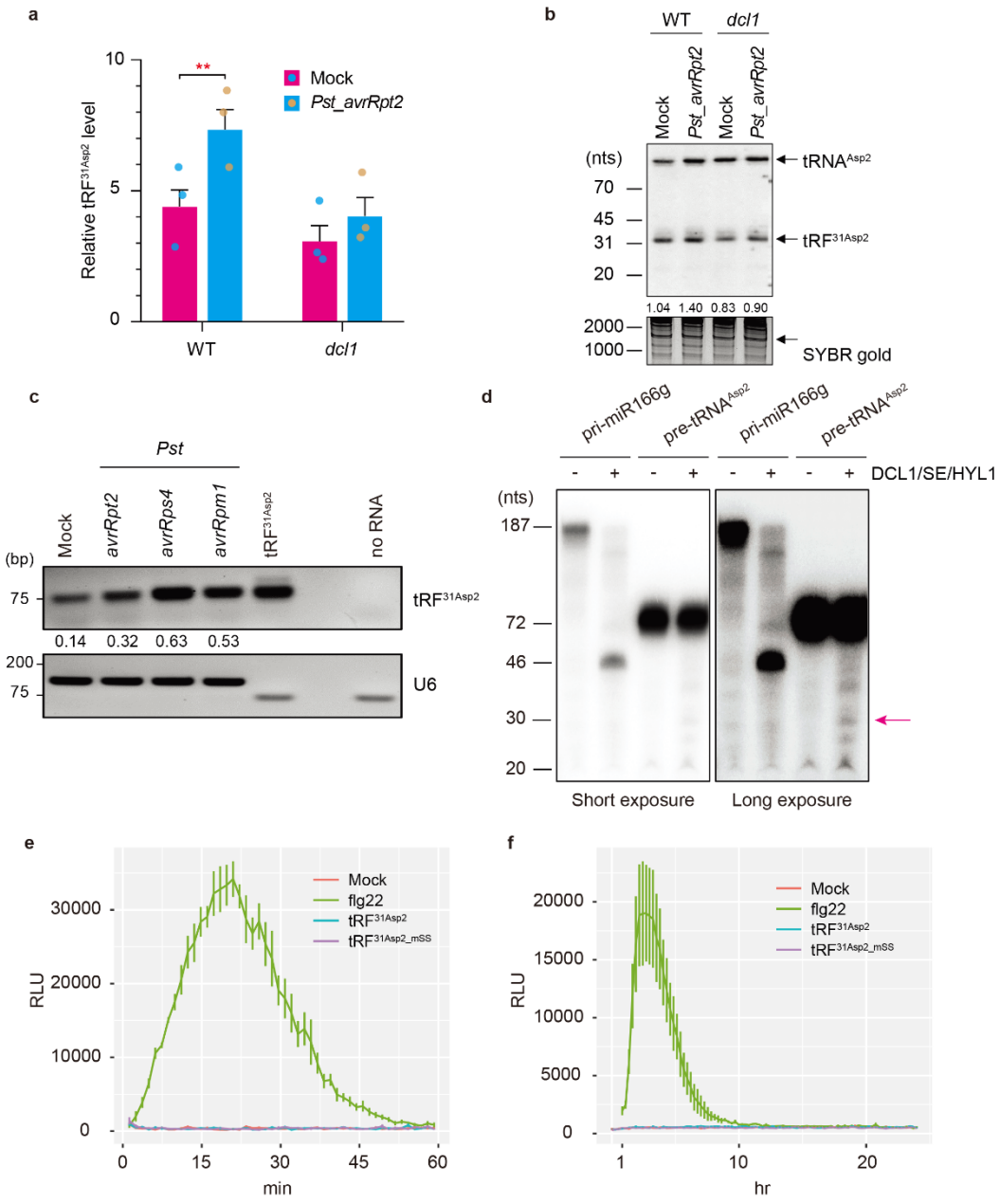

Supplementary Fig. 4 | Measuring the levels of tRF^{31Asp2} using stem-loop RT-PCR and northern blot analysis, examining its *in vitro* cleavage with DCL1, and assessing its changes in reactive oxygen species (ROS). a and b, tRF^{31Asp2} induction by *Pst_avrRpt2* was examined by stem-loop qRT-PCR (a) and northern blot analysis (b) at 1 hpi. **a**, Relative transcription levels in qRT-PCR are presented as the mean±SD (n = 3), and statistical difference between indicated pairs is noted; **P<0.01 (t-test). **b**, The northern analysis of sRNAs was performed with a DIG-labeled probe for tRF^{31Asp2} (upper), while the larger RNAs in the same gel, stained with SYBR gold, are presented as an input marked by an arrow (lower). The values below the northern analysis represent the ratio of tRF^{31Asp2} to the input. **c,** tRF^{31Asp2} induction in WT by three different effectors from *Pst* at 1 hpi was examined by semiquantitative stem-loop RT-PCR. tRF^{31Asp2} and no RNA were used as controls; *U6* was used as an input control. The values between the panels represent the ratio of the target band to the input. **d,** Assessment of DCL1 processing of *in vitro* transcribed a pre-tRNA^{Asp2GTC}. Pri-miR166g was used as a control. Two exposures of the same image were presented side by side. A band close to 31 nts from pre-tRNA^{Asp2GTC} plus DCL1 was indicated with an arrow. On the left side, the sizes of pri-miR166g, its 5'

end processed product, and pre-tRNA^{Asp2GTC} are shown along with two more size markers at 20 and 30 nts. **e and f,** ROS in the leaves of WT treated with water (mock), flg22, tRF^{31Asp2}, or tRF^{31Asp2_mSS} were measured in relative light units (RLU) at the times indicated; the mean±S.E. is presented (n=4). **b,c,d,** Size markers are shown on the left of the panels in kDa or nts.

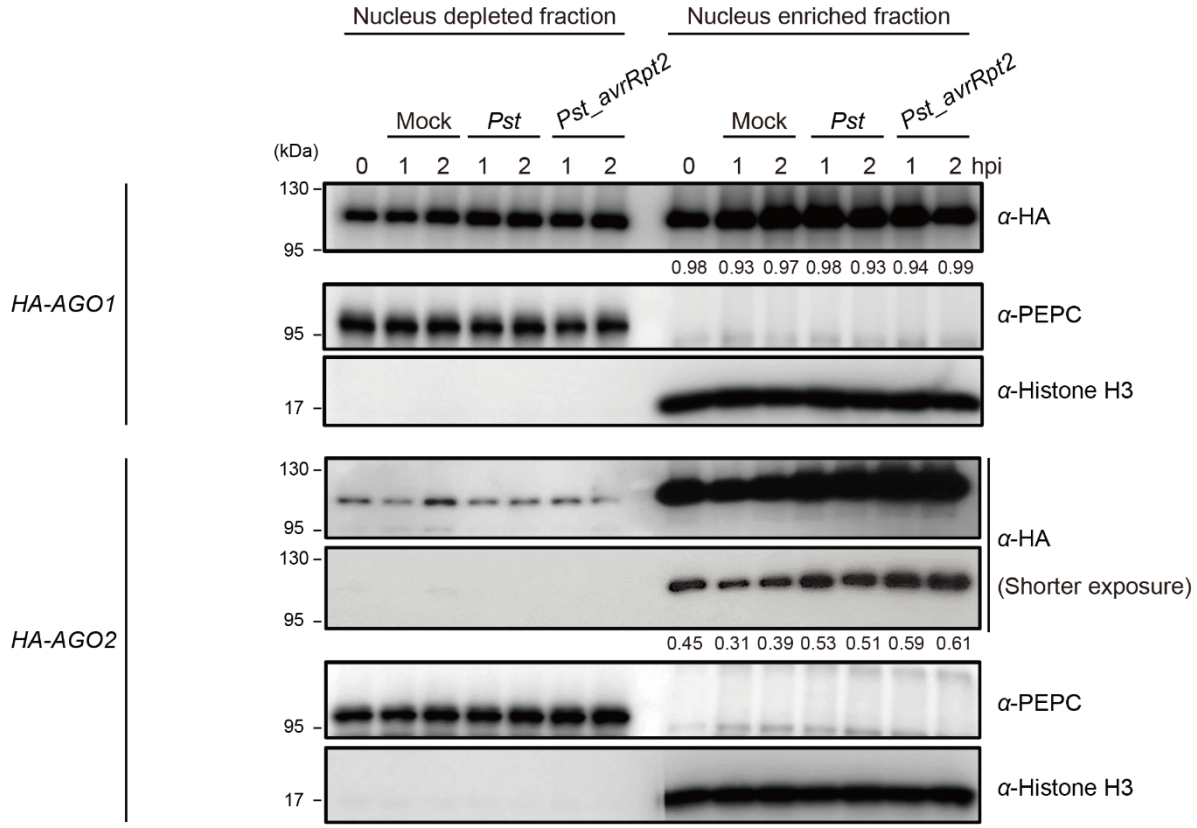

Supplementary Fig. 5 | Subcellular localization of AGO1 and AGO2 in response to *Pst* infection. Leaves from transgenic plants carrying *HA-AGO1* or *HA-AGO2* driven by their own promoters were harvested at 0, 1, and 2 hpi with *Pst*, *Pst_avrRpt2* or mock at 10^6 cfu/ml. Subcellular fractionation was performed to generate nucleus-enriched and -depleted fractions. Immunoblotting (IB) analysis with α-HA was performed to track the AGO proteins; α-phosphoenolpyruvate carboxylase and α-histone H3 were used to ensure depletion or enrichment of nuclei, respectively. Three biological replicates were performed with similar results. The values beneath the α-HA panels represent the quantification of HA, which was normalized using H3 as a reference. Size markers are shown on the left of the panels in kDa. Note that the image at the bottom was not sliced or pasted; we believe the unusual pattern resulted from an artifact, possibly introduced during the transfer process, and included three unedited images with different exposures in Supplementary Fig. 13.

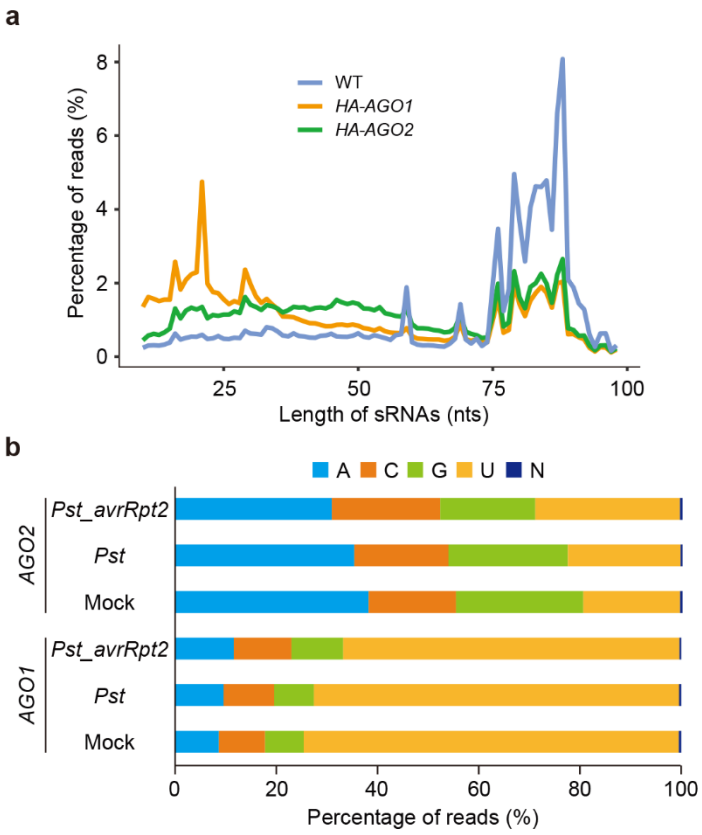

Supplementary Fig. 6 | The size and 5' terminal nucleotide profiles of nuclear AGO1 and AGO2-associated RNAs. a, The size distribution of the sRNAs associated with nuclear AGO1 and AGO2 with WT serving as a control. **b,** The relative frequency of 5' terminal nucleotide of the 21 nts siRNA and miRNA associated with nuclear AGO1 and AGO2.

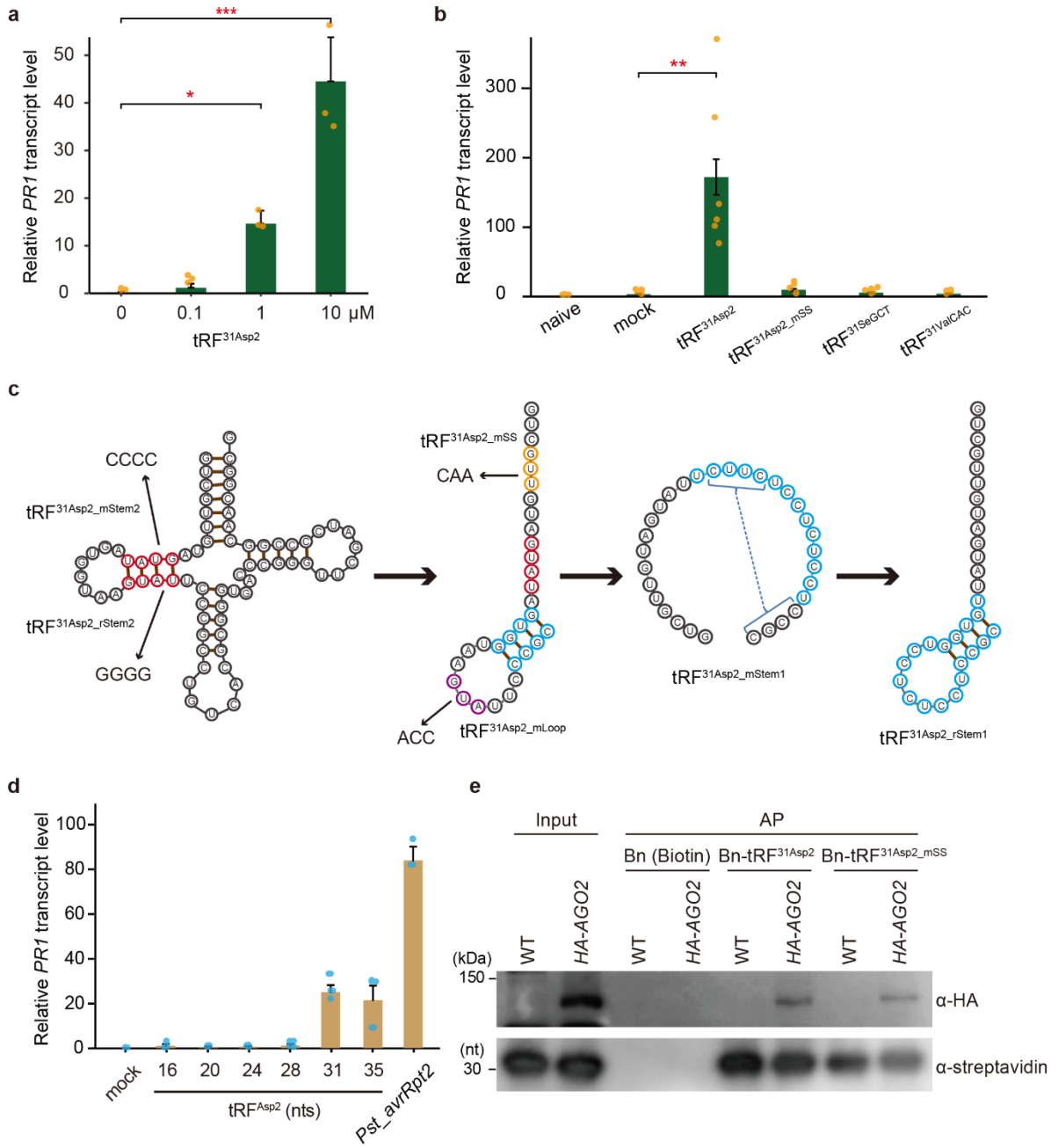

Supplementary Fig. 7 | tRF^{31Asp2} secondary structure is important for its biological activity. a, tRF^{31Asp2} infiltration triggers dose-dependent expression of *PR1*, measured by qRT-PCR. **b,** tRF^{31SerGCT} and tRF^{31ValCAC}, non-induced tRFs, did not induce *PR1*, measured by qRT-PCR at 24 hpi. Relative transcript levels are presented as mean±SE (n ≥4). **c,** Schematic representation of mutations targeting the primary and secondary structure of tRF^{31Asp2}. **d,** *PR1* induction by tRF^{31Asp2} or the 3' addition/deletion mutants was examined by qRT-PCR at 24 hpi; relative transcription levels are presented as the mean±SD (n = 3). **e,** *In vivo* affinity precipitation (AP) assay of *HA-AGO2* transgenic plants with biotin (Bn)-labeled tRF^{31Asp2} or tRF^{31Asp2_mSS}. Input and APed samples were subjected to IB analysis using α-HA and α-streptavidin antibodies. Size markers are shown on the left of the panels in kDa or nt. **a**, **b**, and **d**, **b,c,d,** Statistical difference mock and tRFs is presented; *P<0.05, **P<0.01, ***P<0.001 (t-test).

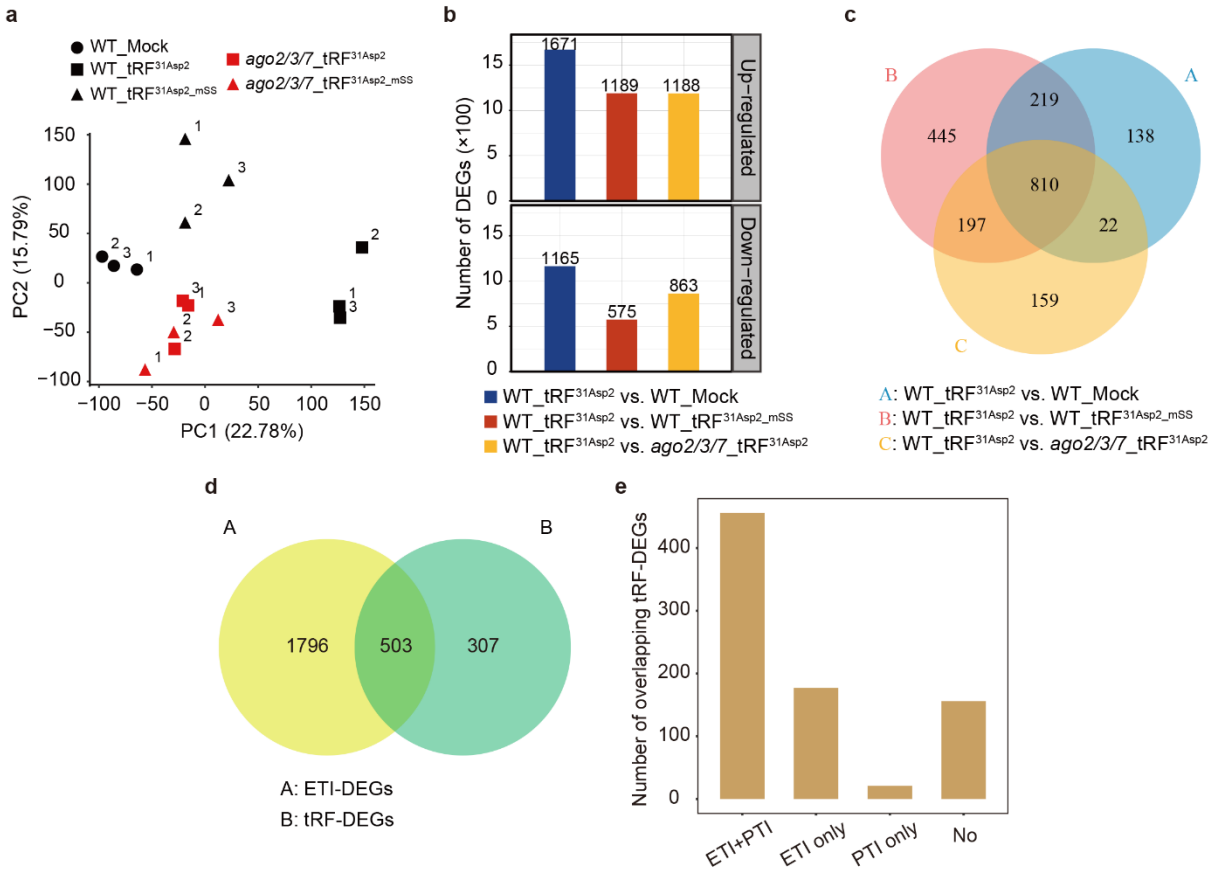

Supplementary Fig. 8 | Most tRF^{31Asp2}-induced DEGs overlap with ETI-induced DEGs. a, Principal component analysis of the normalized RNA-seq data. **b,** The number of induced (upper) and suppressed (lower) DEGs identified by pair-wise comparisons of transcriptomes from WT treated with tRF^{31Asp2} (WT_tRF^{31Asp2}) and: i) WT treated with buffer (mock control; WT_Mock), ii) WT treated with tRF^{31Asp2_mSS} (WT_tRF^{31Asp2_mSS}), or iii) *ago2/3/7* treated with tRF^{31Asp2} (*ago2/3/7*_tRF^{31Asp2}). **c,** Overlap of induced DEGs among the three pair-wise comparisons in **b**. 810 DEGs common to all three comparisons were defined as tRF-DEGs. **d,** Overlap between tRF- and ETI-DEGs. **e,** Many DEGs involved in both ETI and PTI were induced by tRF^{31Asp2}. The classification of DEGs into categories of 'ETI+PTI', 'ETI only', and 'PTI only' was based on a recent study[6], and the extent of overlap between these categories and the tRF-DEGs was counted; The absence of any overlap between tRF-DEGs and the defined DEGs[6] was labeled as 'No'.

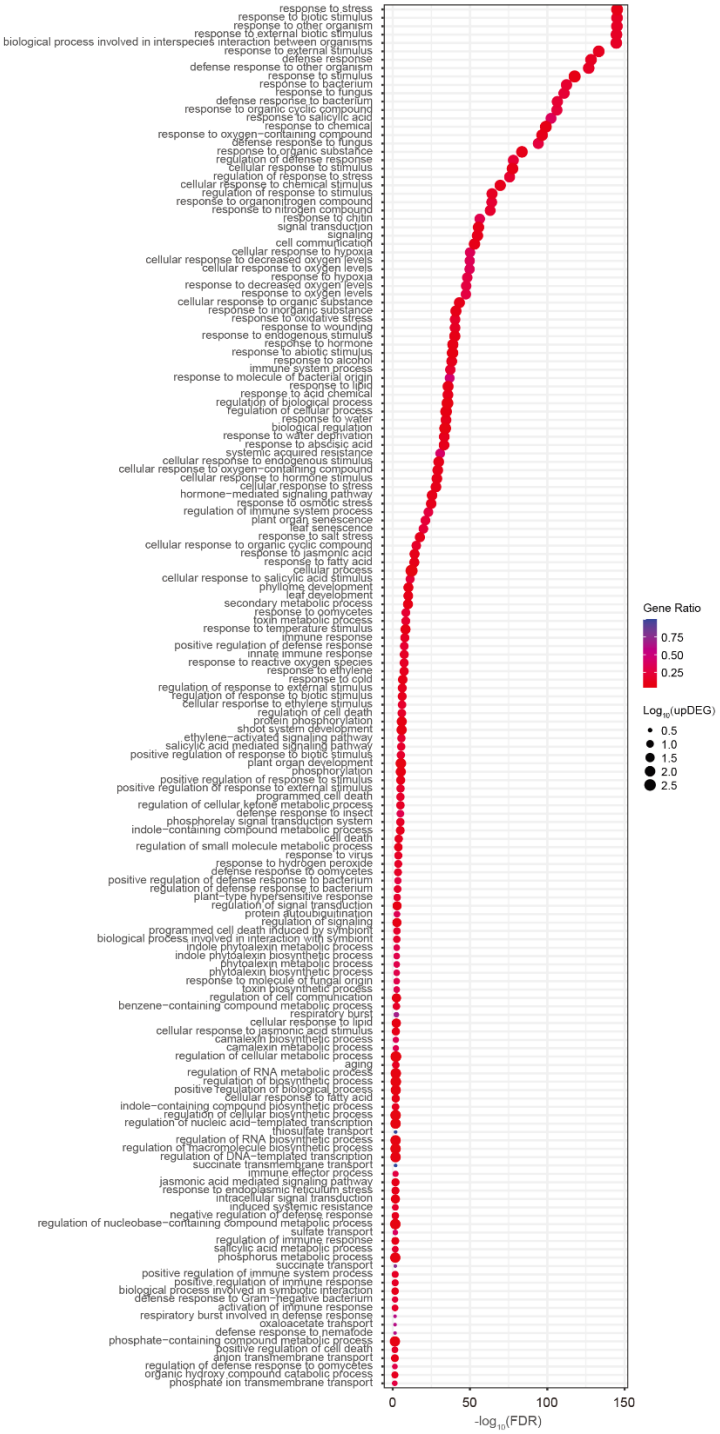

Supplementary Fig. 9 | The GO enrichment analysis of tRF-DEGs. GO enrichment analysis ("biological process" category) of the up-regulated genes shared by ETI treatment and tRF mutation. x-axis: adjusted P-value (FDR, false discovery rate); y-axis: enriched GO term. Dots represent term enrichment. Gene ratio (#significant genes/#annotated genes) indicating the statistical significance of the enrichment is represented along a gradient color from blue (less significant) to red (most significant). The sizes of the dots represent the count of DEGs belonging to each term. Only the significantly enriched GO categories (FDR<0.01) are presented.

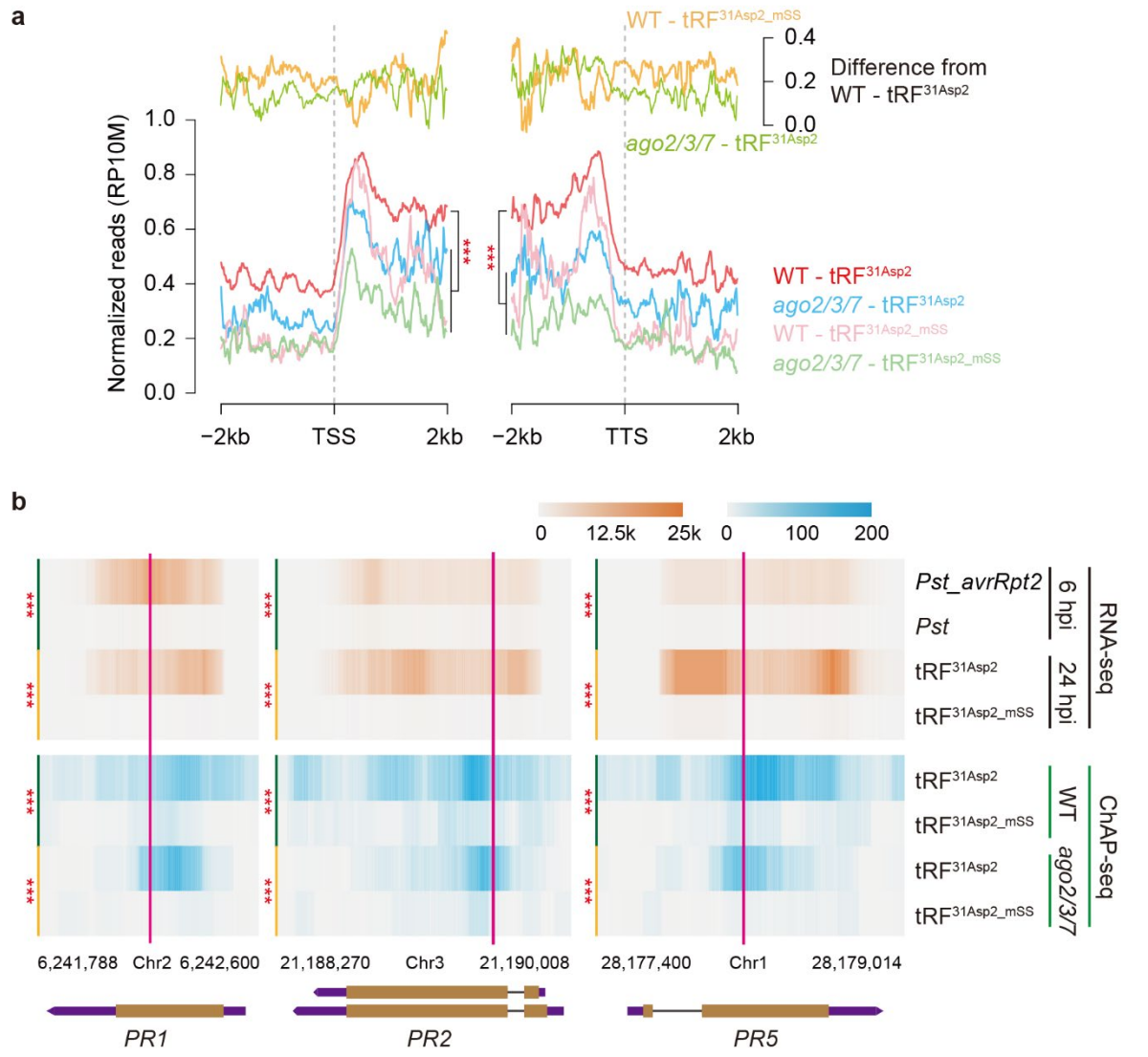

Supplementary Fig. 10 | tRF^{31Asp2} physically associates with genic regions of chromatin. a, The distribution of ChAP-seq reads from regions around the TSS (transcription start sites) and TTS (transcription termination sites) of tRF-DEGs in tRF^{31Asp2}- and tRF^{31Asp2_mSS}-infiltrated WT and *ago2/3/7* plants. Normalized read counts per 10 million (RP10M) were estimated within each 10-bp interval and merged from all four independent batches. The differences between tRF^{31Asp2} and tRF^{31Asp2_mSS} in WT are presented in yellow, while those between tRF^{31Asp2} in WT and *ago2/3/7* are shown in green. **b,** Read-density heatmap of indicated RNA-seq and ChAP-seq analyses for *PR1*, *PR2,* and *PR5*. Sites carrying a sequence homologous to tRF^{31Asp2} are denoted with a red line. Significance for indicated pairs is noted; ***P<0.001 (Wilcoxon rank sum test).

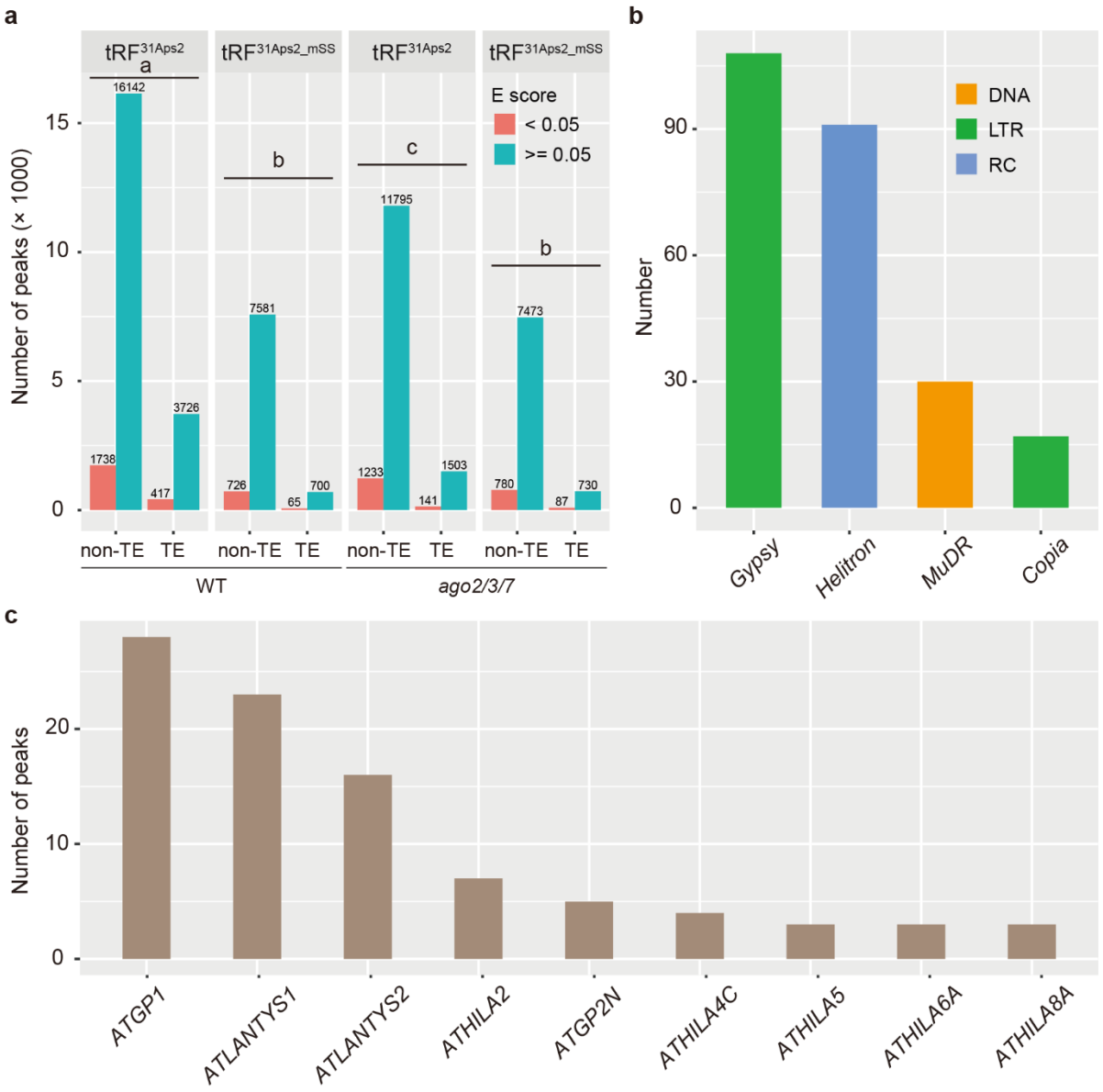

Supplementary Fig. 11 | Distribution of tRF^{31Asp2} binding sites and their association with *Gypsy* LTR-retroposons. a, The number of ChAP-seq peaks overlapping with transposon (TE) and non-transposon regions (non-TE) in WT and *ago2/3/7*. The binding sites were further categorized based on their sequence similarity to tRF^{31Asp2} using the E score. Different letters above each group denote significant difference ($P<10^{-7}$; Fisher's LSD post-hoc test). **b,** The number of ChAP-seq peaks that also contain the tRF^{31Asp2} binding sequence in each transposon superfamily. **c,** The number of ChAP-seq peaks that also contain the tRF^{31Asp2} binding sequence in different members of the *Gypsy* retrotransposon superfamily from **(b)**.

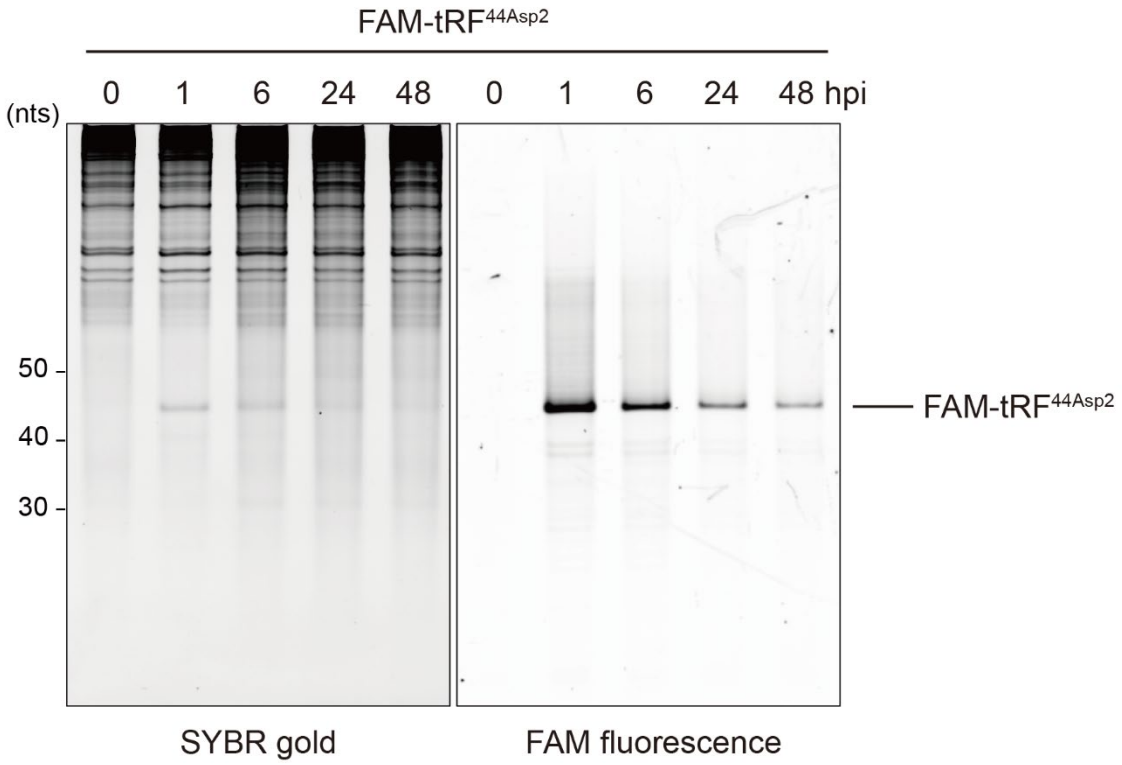

Supplementary Fig. 12 | Leaf transfection with synthetic tRF RNA oligonucleotides leads to nuclear localization. Nuclear RNA from WT plants infiltrated with a 1 µM of 5' 6-fluorescein (FAM)-conjugated tRF^{44Asp2} oligonucleotide was isolated at the indicated time points. Extracted RNAs were separated in 15% PAGE with 8 M urea and detected by SYBR gold staining and FAM-specific fluorescence scanning. Size markers are shown on the left of the panels in nt.

Supplementary Fig. 13 | Uncropped Images

Supplementary Figure 4c (uncropped)

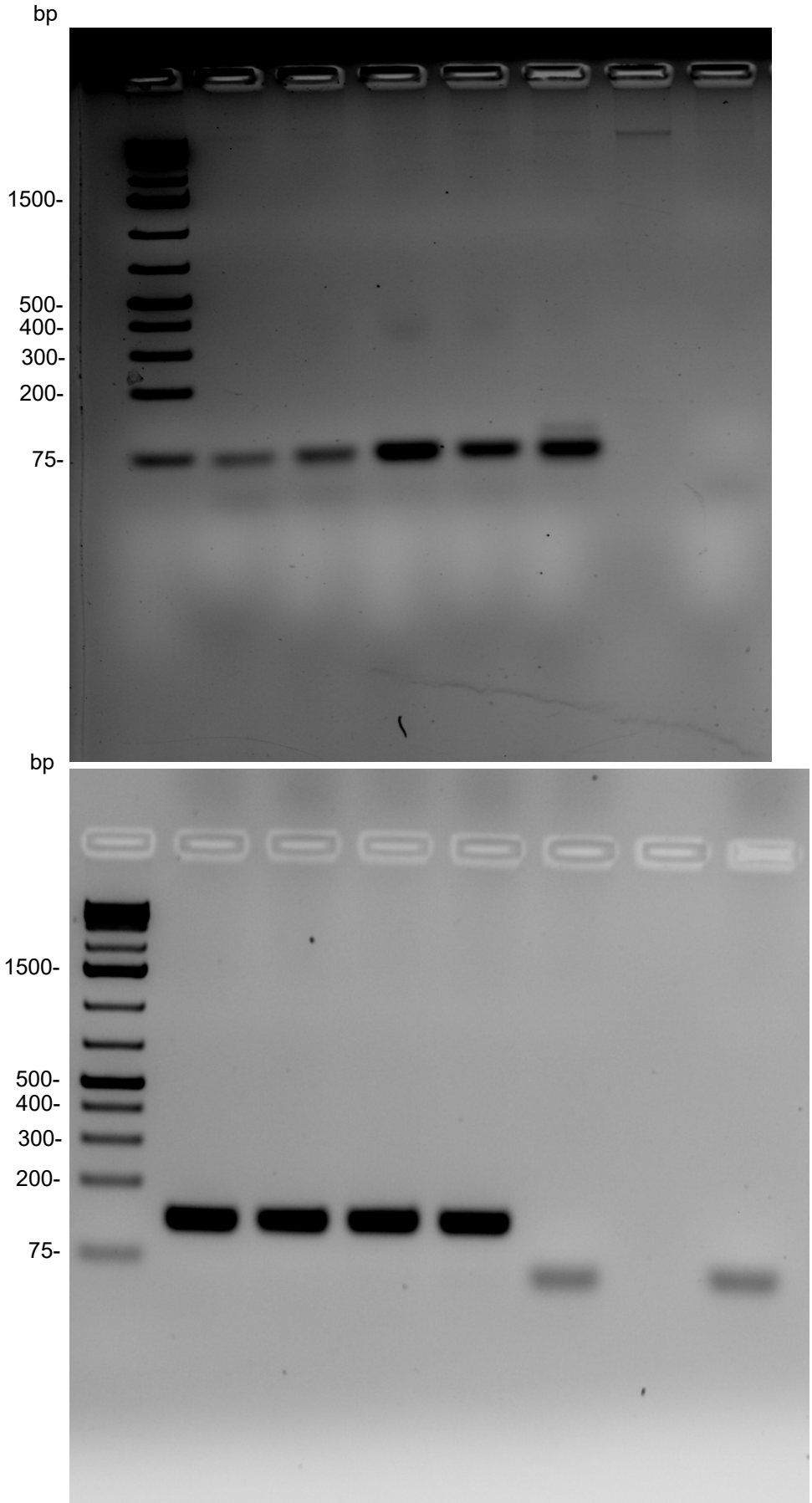

Supplementary Figure 5 (uncropped)

Anti-HA (AGO1)

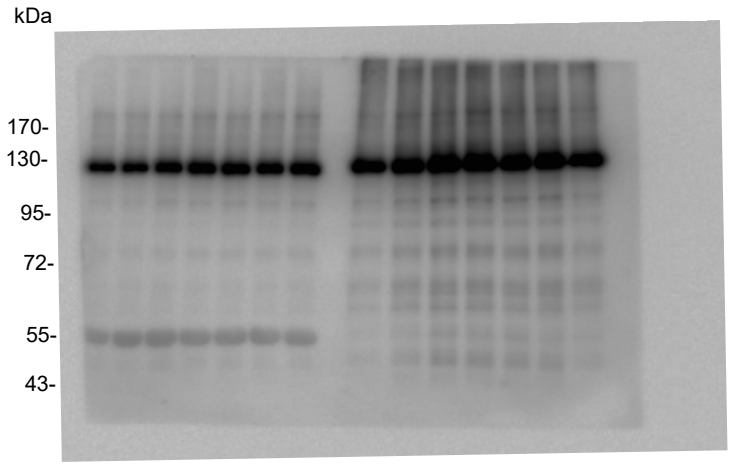

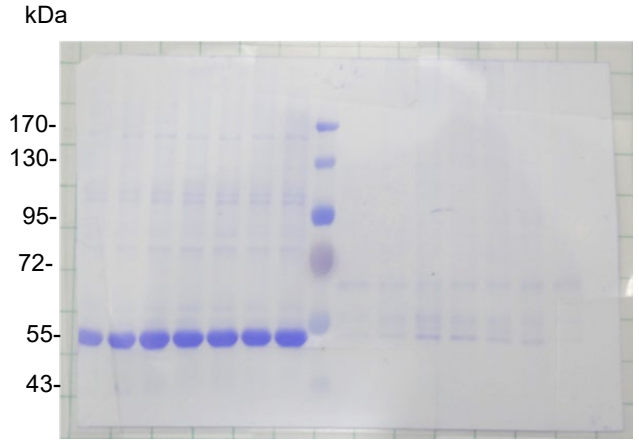

Anti-Histone (AGO1)

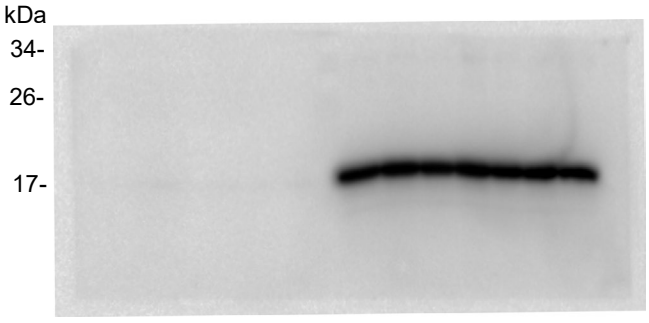

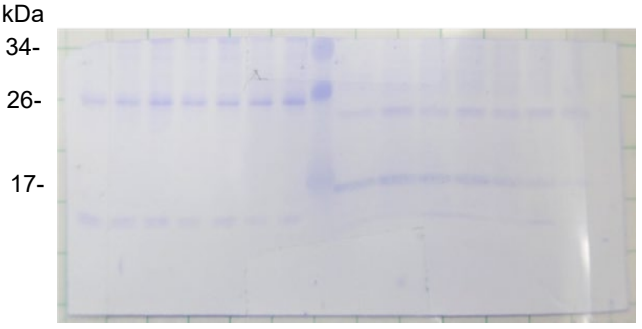

Anti-PEPC (AGO1)

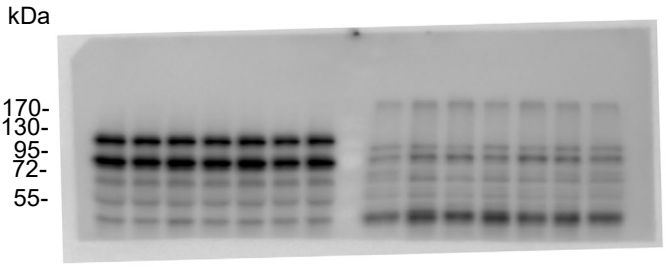

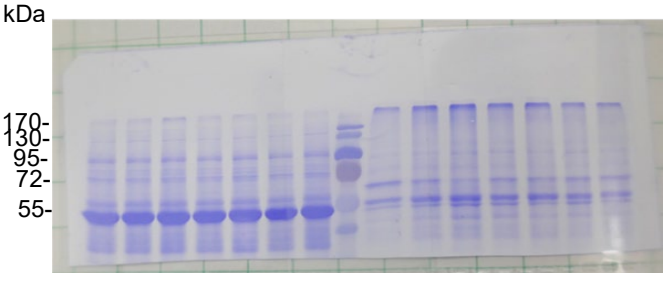

Anti-HA (AGO2)

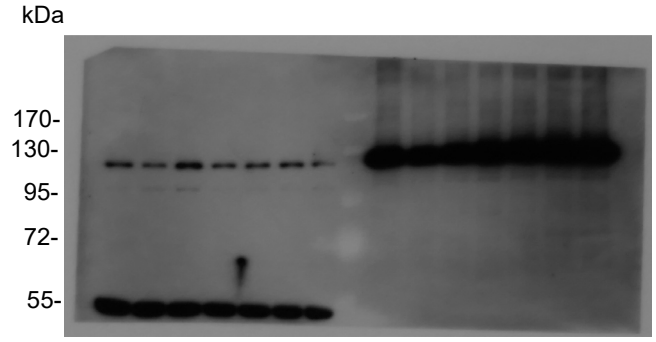

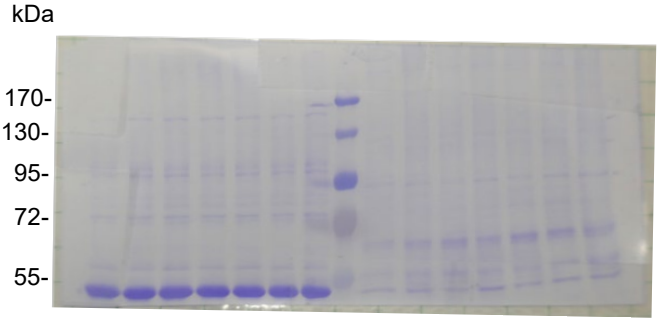

Long exposure

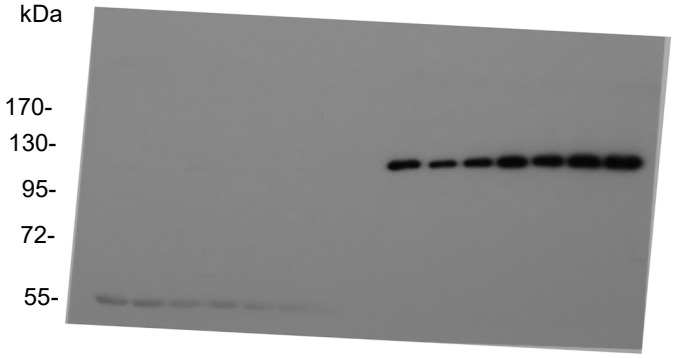

Short exposure

Anti-Histone (AGO2)

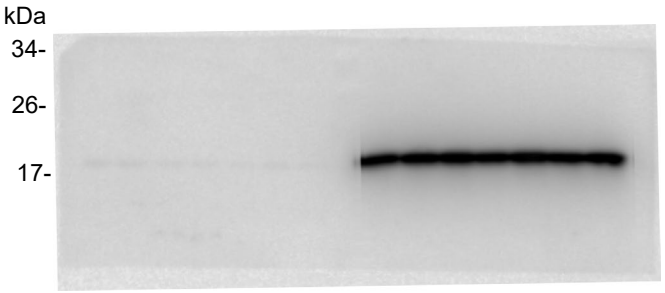

Anti-PEPC (AGO2)

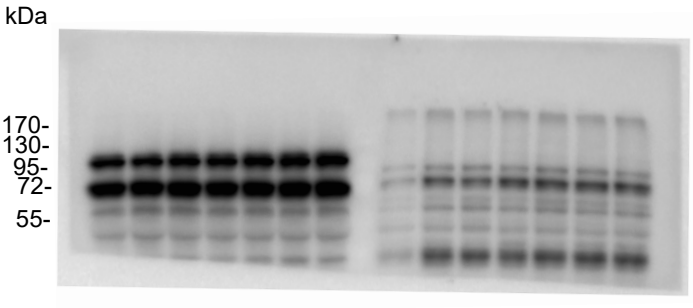

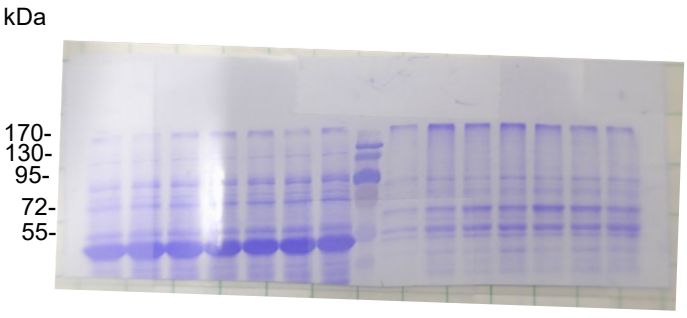

Anti-Histone (AGO2):
Different exposures

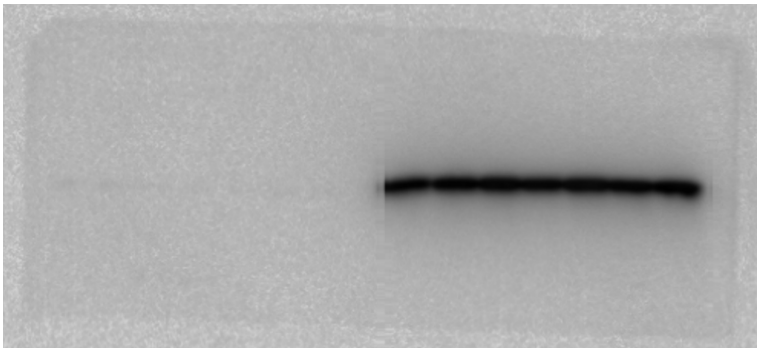

10sec

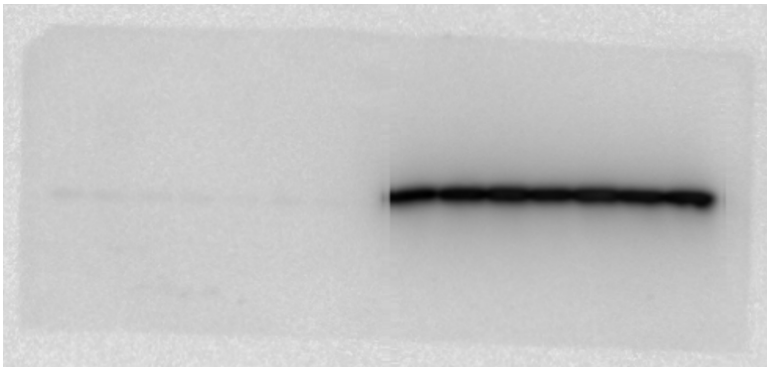

20sec

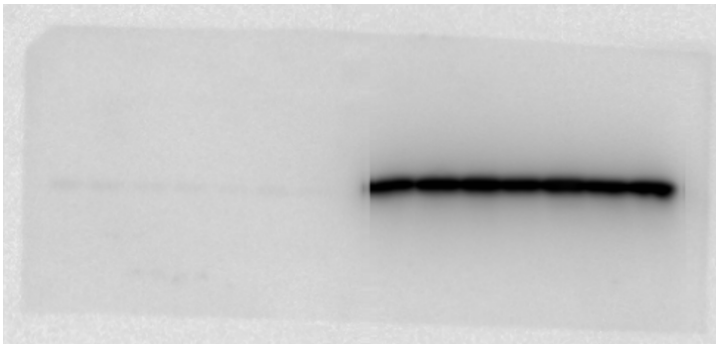

30sec

Supplementary Figure 7e (uncropped)

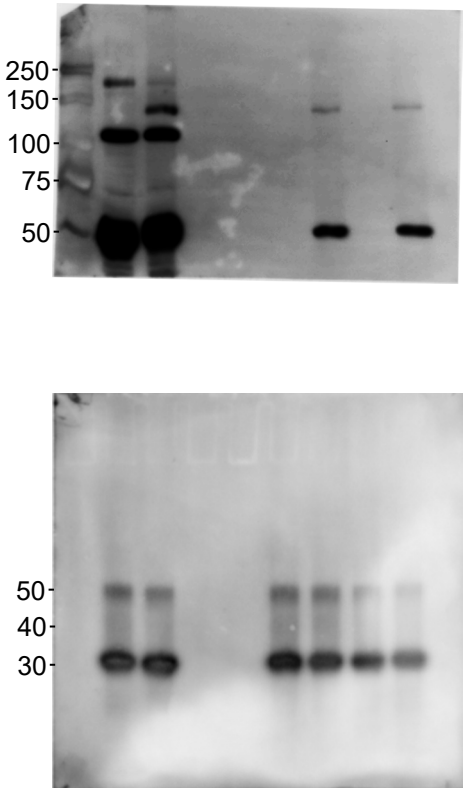

Supplementary Figure 12 (uncropped)

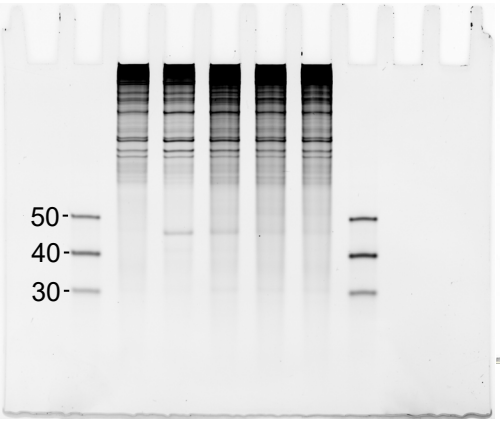

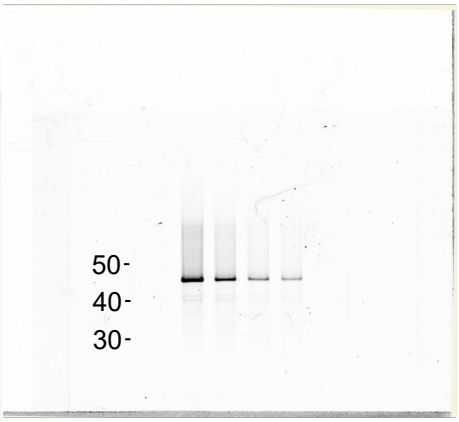

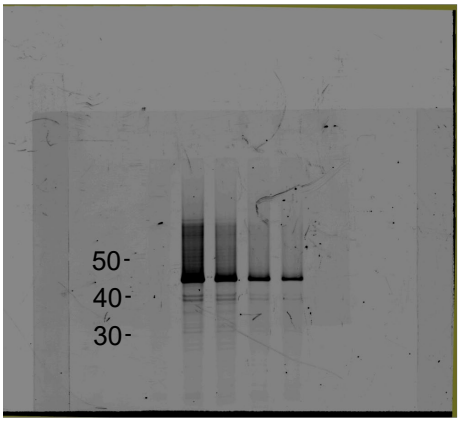

Supplementary Table 1. List of oligos used in this study.		
Name	**Sequence**	**Purpose**
RT-Tip41_F	GGATACCCTTTCGCAGATAGAGAC	qRT-PCR
RT-Tip41_R	GCGATTTTGGCTGAGAGTTGAT	
RT-RHIP1_F	CACTAGGCCGATTTCAGAGC	
RT-RHIP1_R	CCATCAAATCAGCAGCTTCA	
RT-PR1_F	CCACCATTGTTACACCTCACTTT	
RT-PR1_R	AAAACTTAGCCTGGGGTAGCGG	
tRF^{16Asp2}	[Phos]GGGAUUGUAGUUCAAU	tRF transfection
tRF^{20Asp2}	[Phos]GGGAUUGUAGUUCAAUCGGU	
tRF^{24Asp2}	[Phos]GGGAUUGUAGUUCAAUCGGUCAGA	
tRF^{28Asp2}	[Phos]GGGAUUGUAGUUCAAUCGGUCAGAGCAC	
tRF^{35Asp2}	[Phos]GGGAUUGUAGUUCAAUCGGUCAGAGCACCGCCCUG	
tRF^{31Asp2}	[Phos]GUCGUUGUAGUAUAGUGGUAAGUAUUCCCGC	
tRF^{31Asp2_mSS}	[Phos]GUCCAAGUAGUAUAGUGGUAAGUAUUCCCGC	
tRF^{31Asp2_mStem1}	[Phos]GUCGUUGUAGUAUucuucuccucuccuCCGC	
tRF^{31Asp2_rStem1}	[Phos]GUCGUUGUAGUAUuGUGGuccucuccuCCGC	
tRF^{31Asp2_mStem2}	[Phos]GUCGUUGUAGUAUAGUGGUAAccccUCCCGC	
tRF^{31Asp2_rStem2}	[Phos]GUCGUUGUAGgggAGUGGUAAccccUCCCGC	
$tRF^{31SerGCT}$	[Phos]GGAGGGAUGGCUGAGUGGCUUAAGGCAUUGG	
$tRF^{31ValCAC}$	[Phos]GUCUGGGUAGUGUAGUCGGUUAUCACGCUAG	
tRF^{31Asp2_mLoop}	[Phos]GUCGUUGUAGUAUAGUGGUAAaccUUCCCGC	
RC_tRF^{31Asp2}	GCGGGAATACTTACCACTATACTACAACGAC	
$RC\_tRF^{31Asp2\_mSS}$	GCGGGAATACTTACCACTATACTACTTGGAC	
$FAM\text{-}tRF^{44AspGTC}$	[6FAM]GGGAUUGUAGUUCAAUCGGUCAGAGCACCGCCCUGUCAAGGCGG	
$Biotin\text{-}tRF^{31Asp2}$	[Btn]GUCGUUGUAGUAUAGUGGUAAGUAUUCCCGC	ChAP-seq
$Biotin\text{-}tRF^{31Asp2\_mSS}$	[Btn]GUCCAAGUAGUAUAGUGGUAAGUAUUCCCGC	

STTM_F_tRF^{31Asp2}	gccATTTAAATatggtctaaagaagaagaatGCGGGAATACTTACCACTATActaCTACAACGACgaattcggtacg ctgaaatcaccag	STTM lines
STTM_R_tRF^{31Asp2}	gccATTTAAATtagaccataacaacaacaacGTCGTTGTAGtagTATAGTGGTAAGTATTCCCGCaagcttgggctg tcctctccaaatg	
STTM_F_tRF^{31Asp2_mSS}	gccATTTAAATatggtctaaagaagaagaatGCGGGAATACTTACCACTATActaCTACTTGGACgaattcggtacg ctgaaatcaccag	
STTM_R_tRF^{31Asp2_mSS}	gccATTTAAATtagaccataacaacaacaacGTCCAAGTAGtagTATAGTGGTAAGTATTCCCGCaagcttgggct gtcctctccaaatg	
pT7-tRNA_AspGTC_F	GATCACTAATACGACTCACTATAGTCGTTG	*in vitro* transcription of tRNA^{Asp2}
tRNA_AspGTC_R	CGCCGTTGCCGGGGATCG	
pT7- F	GATCACTAATACGACTCACTATA	
cDNA_Stem_tRF^{31Asp2}_R2	GTTGGCTCTGGTGCAGGGTCCGAGGTATTCgcaccagagccaacGCGGGAATAC	Stem-loop qRT
cDNA_Stem_U6_R	GTTGGCTCTGGTGCAGGGTCCGAGGTATTCgcaccagagccaacCCAAAAAAAATTTG	
RT_tRF^{31Asp2}_F	CGGGTCGTTGTAGTATAGTGGTAAGTAT	
RT_Stem_U6_F	GGGGACATCCGATAAAATTGG	
RT_Stem_Univ_R	GTGCAGGGTCCGAGGTATTC	
DIG LNA-DNA probe	[DIG] CTTACCACTATAC[+T] [+A] [+C] [+A] A[+C] [+G] [+A] C	Northern blot; LNA-modified nucleotide is noted as [+]

Supplementary Table 2. List of reagents used in this study		
Reagent	**Vendor**	**Catalog Number**
Goat polyclonal anti-HA-HRP	ThermoFisher Scientific	NB600362H
Polyclonal HRP-streptavidin	ThermoFisher Scientific	N200
Rabbit polyclonal anti-Histone H3	Abcam	ab1791
Rabbit polyclonal anti-phospho enol pyruvate carboxylase	Rockland	200-4163
Goat Anti-Rabbit IgG H&L (HRP)	Abcam	ab97051
30% Acrylamide/Bis Solution,37.5:1	BioRad	1610158
40% Acrylamide: Bis-Acrylamide 29:1	ThermoFisher Scientific	BP1408-1
5x HOT FIREPol EvaGreen qPCR Mix Plus	Solis BioDyne	08-24-0000S
Absolute ethanol	ThermoFisher Scientific	BP2818500
Acetic Acid	ThermoFisher Scientific	A38S-500
Amersham Hybond-N+	ThermoFisher Scientific	45-000-850
Ammonium persulfate	ThermoFisher Scientific	50-899-90040
Autoradiography GBX developer	Sigma-Aldrich	P7042-5GA
Autoradiography GBX fixer	Sigma-Aldrich	P7167-5GA
Chloroform	ThermoFisher Scientific	BP1145-1
D-(+)-Biotin	ThermoFisher Scientific	AAA1420703
D1000 Reagents	Agilent Technologies	5067-5583
Diethylpyrocarbonate	ThermoFisher Scientific	ICN15090205
Dithiotritol	ThermoFisher Scientific	BP172-5
DNase I	NEB	M0303L
Dynabeads™ M-280 Streptavidin	ThermoFisher Scientific	11205D
Ethanol	ThermoFisher Scientific	BP2818
Ethidium Bromide	ThermoFisher Scientific	15585011
Ethylenediaminetetraacetic Acid	ThermoFisher Scientific	S311-500
EZview™ Red Anti-HA Affinity Gel	Millipore Sigma	E6779-1ML
Formamide	ThermoFisher Scientific	bp227-100
Glycine	ThermoFisher Scientific	BP381-5
HA Peptide	Genscript	RP11735-5
HEPES	ThermoFisher Scientific	11344041
Isopropanol	ThermoFisher Scientific	BP2618-500
Magnesium Chloride Hexahydrate	ThermoFisher Scientific	M33-500
Methanol	ThermoFisher Scientific	A452-4

MIRACLOTH	Sigma-Aldrich	475855-1R
M-MuLV Reverse Transcriptase	NEB	M0253L
Phenylmethanesulfonyl fluoride	Sigma-Aldrich	P7626-25G
Pipes	ThermoFisher Scientific	ICN19483880
Protease inhibitor cocktail	ThermoFisher Scientific	78437
Proteinase K	NEB	P8107S
PVDF Membrane	ThermoFisher Scientific	HVLP02500
RNase A	ThermoFisher Scientific	FEREN0531
RNase Inhibitor	NEB	M0307
Sodium Chloride	ThermoFisher Scientific	02-004-049
Sodium Dodecyl Sulfate	ThermoFisher Scientific	BP166-500
Sucrose	Sigma-Aldrich	S8501-5KG
SYBR gold	ThermoFisher Scientific	s-11494
T4 Polynucleotide Kinase	NEB	M0201S
TEMED	ThermoFisher Scientific	BP150-20
Tris Base	ThermoFisher Scientific	BP152-5
Triton X-100	Sigma-Aldrich	9002-93-1
Trizol Reagent	ThermoFisher Scientific	15596018
Tween 20	ThermoFisher Scientific	BP337-500
Urea	ThermoFisher Scientific	bp169-500
EMD Millipore™ Amicon™ Ultra-0.5 Centrifugal Filter Units	ThermoFisher Scientific	UFC501024
mirVana™ miRNA Isolation Kit	ThermoFisher Scientific	am1561
NEBNext Poly(A) mRNA Mag Isolation	NEB	E7490L
NEBNext® Ultra™ II RNA Library Prep Kit for Illumina	NEB	E7770
NEBNext® Multiplex Oligos for Illumina® (Dual Index Primers Set 1)	NEB	E7600S
NEBNext® Ultra™ II DNA Library Prep kit	NEB	E7103
QIAseq miRNA Library Kit	Qiagen	331502
QIAseq miRNA NGS 48 Index IL	Qiagen	331595
Qubit dsDNA HS Assay Kit	ThermoFisher Scientific	Q32854
Qubit RNA HS Assay Kit	ThermoFisher Scientific	Q32855
Qubit microRNA Assay Kit	ThermoFisher Scientific	Q32880
ECL 2 Western Blotting Substrate	ThermoFisher Scientific	PI80196
Flagelin22	Genscript	RP19986
Luminol	Sigma-Aldrich	A85111

Horse Raddish Peroxidase (type VI-A)	Sigma-Aldrich	P6782
nylon membrane	Roche	209299001
EDC	Sigma	7750
anti-DIG antibody	Roche	11093274910
CSPD	Roche	11655884001
DreamTaq DNA Polymerase	ThermoFisher Scientific	EP0703
MagnaBind™ Goat Anti-Rabbit IgG	ThermoFisher Scientific	21356